Scalable multi-material additive manufacturing of bioinspired polymeric material with metallic structures via electrically assisted stereolithography

4 5 6

1

2

3

Tengteng Tang

- 7 Department of Aerospace and Mechanical Engineering, School for Engineering of Matter,
- 8 Transport and Energy
- 9 Arizona State University, Tempe, AZ 85281
- 10 ttang32@asu.edu

11 12

Bhushan Ahire

- 13 Department of Aerospace and Mechanical Engineering, School for Engineering of Matter,
- 14 Transport and Energy
- 15 Arizona State University, Tempe, AZ 85281
- 16 bahire@asu.edu

17

18 Xiangjia Li¹

- 19 Department of Aerospace and Mechanical Engineering, School for Engineering of Matter,
- 20 Transport and Energy
- 21 Arizona State University, Tempe, AZ 85281
- 22 xiangjia.li@asu.edu
- 23 ASME Membership:000102217951

242526

ABSTRACT

- Heterogeneous material systems consisting of metallic structures and polymer matrixes are of significance
- for applications such as integrated circuits, microelectromechanical devices, antennas, sensors, actuators,
- 30 and metamaterials. Scaly-foot snail which lives in the deep ocean exhibits high strength and temperature
- 31 resistance due to unique shells made of metal and polymer. Recently, different multi-material structures
- 32 have been fabricated with metal deposition using multiple manufacturing processes. However, using these

¹ Corresponding author.

complicated hybrid processes is challenging to construct complex 3D structures of heterogeneous material with enhanced properties, high resolution, and time efficiency. Here, we establish a novel manufacturing strategy to build bioinspired hierarchical structures with heterogeneous material systems using electrically assisted stereolithography. The photocurable printing solution that can act as an electrolyte for charge transfer was developed, and the curing characteristic of the printing solution was further investigated. A fundamental understanding of the formation mechanism of metallic structures on the polymer matrix was studied through physics-based multiscale modeling and simulations. The correlation between metallic structures morphology, printing solution properties, and printing process parameters, and their effects in building bioinspired hierarchical structures with heterogeneous materials were identified. Demonstrative test cases were built to verify the printing performance of the proposed approach. This research work will deliver a scalable AM process that can facilitate various interesting applications based on bioinspired heterogeneous material and structures.

INTRODUCTION

Nature organisms have evolved complex hierarchical architectures with highly integrated material, structures, and function over millions of years of evolution and provide guidance for designing high-performance functional devices. Biomimicry opens up an unprecedented path for the design and manufacture of functional devices with excellent mechanical, electromagnetic, and hydrodynamic properties. Meantime AM breaks through the barriers of traditional manufacturing methods and makes bionic manufacturing possible [1]. For example, a scaly-foot snail that lives in the deep-sea hydrothermal vent has attracted the attention of scientists because of its metallic outer surface (Fig.1a). The outer layer of its shell is mainly composed of the iron sulfide-based layer containing greigite, Fe $_3$ S $_4$ with a thickness of about 30 µm, as shown in Fig.1b [2].

59

60

61

62

63

64

65

66

67

68

69

70

71

72

73

74

75

76

77

78

79

This substance does not exist in the skeleton of any other species, which gives its shell extreme hardness and excellent high-temperature resistance. Due to these extraordinary properties, heterogeneous material systems based on metallic structures and polymer matrixes have become a promising research field because of their potential applications in protecting [3], energy dispersion [4], sensing [5, 6], and microelectron-mechanical systems [7]. However, how to bio-mimic such scaly-foot snail for properties enhancement remains to be further studied by using current manufacturing technologies. Benefitting from the proposal of different three-dimensional (3D) printing technologies and widely available printing materials, additive manufacturing (AM) expands its function from simple prototype verification to mass production of highly functional devices [8]. Stereolithography (SL) is one of the most widely used AM technologies for fabricating multi-material and multi-scale structures [9]. Different from extrusion-based printing technologies, such as FDM(fused deposition modeling) or DIW(direct ink writing), photosensitive liquid resin become solid after being irradiated by a certain wavelength of light in the SL process, and the resin is cured layer by layer to obtain a three-dimensional structure [9]. Hence, SL is suitable for the production of microscale complex three-dimensional structure and is characterized by high resolution, cross-scale processing, high processing efficiency, and low processing cost [1]. However, there is a main obstacle that how is to print metallic materials with polymer matrix all at once rather than the normal multiple processes-based manufacturing approach, especially using electrodepositing to fabricate metallic structures with conductive polymers.

81

82

83

84

85

86

87

88

89

90

91

92

93

94

95

96

97

98

99

100

101

By integrating with AM processes, various hybrid metallization technologies have recently emerged to solve the challenges as mentioned above. For example, Hudkins et al. demonstrated that conductive PLA/carbon polymer composites could be used to print electrodes, and 3D printed objects were then electroplated with nickel [10]. Rosa-Ortis et al. used the same kind of commercially available composite filament to fabricate conductive 3D parts and further coated metal layers by employing hydrogen assisted electroplating (HAE) method [11]. Lazarus et al. utilized dual extruder heads filled with conductive PLA/copper and nonconductive ABS filament to print 3D objects and then selectively electroplate the conductive domain to build 3D circuit boards [12]. Similar research was carried out by using conductive and nonconductive filaments to print 3D parts, and then 3D metallic structures was selectively electroplated on the conductive areas of 3D printed objects [13]. Moreover, Ryan et al. printed 3D structures with a programmable mosaic of surface charge region using mask image projection-based stereolithography (MIP-SL). It allows selective deposition of single metals for multimaterial fabrication of electronic devices [14]. The methods above are multiple processes that are complicated and time-consuming. Besides, the plated layer is not firmly adhered on the printed objects, which increases problems associated with hardenability, nonuniform microstructures, as well as cracking. Researchers carried out extensive work to develop new processes that can print metal/polymer structures in a single step to improve the fabrication efficiency. For instance, Zhao et al. developed a room temperature metal/polymer printing process based on polymer-assisted photochemical deposition. In this process, silver, gold, and platinum can be fabricated on various substrates [15].

103

104

105

106

107

108

109

110

111

112

113

114

115

116

117

118

119

120

121

122

123

Similarly, metallic silver was printed on the polymer substrates using visible light projection lithography at room temperature [16]. However, only certain types of metals and metal/polymer hybrid structures can be printed using current photochemical deposition-based 3D printing.

To solve the current challenges in the 3D printing of heterogeneous materials systems consisting of metal and polymer at room temperature, we put forward a novel process named electrical field-assisted heterogeneous material printing (EF-HMP) that can control the metallic structures deposition on the polymer matrix composite for enhanced functional characteristics. The proposed process aims to fabricate metallic structures in a single step at room temperature, which is difficult by using currently available techniques. In this work, a polymer matrix-based composite that can act as an electrolyte was developed to maintain the metallic ions transport and promote metal deposition on the photocured polymer matrix. To increase the electrical conductivity of photocurable resin, poly(3,4-ethylenedioxythiophene)-poly(styrenesulfonate) (PEDOT:PSS) were mixed with poly(ethylene glycol) diacrylate (Mn 700) (PEGDA), which is widely used in the fabrication of flexible sensors due to its biocompatibility [6, 17]. Besides, the inorganic compounds were added to provide enough metal ions for the deposition. Then we further investigate properties of the newly developed printing solution, including exposure time, curing depth, viscosity, and resistivity. After that, the electrical field generation module was designed and integrated with MIP-SL for the metal deposition. The metallic structures can grow on the cured polymer matrix during the printing process by controlling the electrical field. The deposition of metallic structures is determined by the metal ion concentration,

electrical field voltage, deposition time. In order to achieve accurate printing of polymer/metal material system with desired geometric shapes, the process parameters were optimized based on physics-based modeling, simulation, and testing. The relation between geometric morphology, material properties, and printing process parameters was identified to establish a route to build the scaly-foot snail-inspired heterogeneous materials system with complex 3D shapes. The printing results demonstrate that the proposed EF-HMP process provides a novel manufacturing tool for heterogeneous materials fabrication, which show enormous potential in fabricating devices for various applications in flexible sensor, energy harvest, healthcare, and robotics.

2 MATERIALS AND METHODS

2.1 Materials

Poly(ethylene glycol) diacrylate (Mn 700) (PEGDA), highly conductive poly (3, 4-ethylenedioxythiophene)-poly (styrenesulfonate) (PEDOT:PSS) in pure pellet with 3.0-4.0% H₂O, and Irgacure 819 photoinitiator were purchased from Sigma-Aldrich, St. Louis, MO, USA, and used as received. Copper (II) sulfate (CuSO₄) in crystal form is purchased from Factory Direct Chemicals, Copiague, NY, USA. The deionized water was purchased from DS Services of America, Atlanta, GA, USA.

2.2 Preparation of photocurable electrolyte solution

The photocurable electrolyte solution is composed of a photocurable matrix and conductive fillers. Firstly, the photocurable matrix of 3D printable conductive composite

147

148

149

150

151

152

153

154

155

156

157

158

159

160

161

162

163

164

165

166

167

consisted of PEGDA and PEDOT:PSS used to study curing characteristics, viscosity, and resistivity was prepared by mixing 45 wt% of PEGDA with 2 wt% Irgacure 819 photoinitiator. Different ratio of pellet formed PEDOT:PSS (1 wt%, 3 wt%, 5 wt%, 6 wt%, 8 wt%, and 10 wt%) was dissolved in the remaining proportion of 1 mol/L CuSO₄ solution by stirring at 200 rpm for 0.5 h at room temperature (25°C). Then, the conductive PEDOT:PSS fillers and CuSO₄ solution were added into the photocurable PEGDA matrix, and the solution was stirred at 200 rpm for 1.5h at 25°C. Finally, the prepared photocurable electrolyte solutions were degassed using a vacuum chamber to remove air bubbles for the fabrication. After testing, the optimized composition of the photocurable electrolyte solution used for printing and electrodeposition is 32.5 wt% of PEGDA, 2 wt% of Irgacure 819 photoinitiator, 2 wt% PEDOT:PSS, 35 wt% of 1mol/L CuSO₄ solution, and 28.5 wt% of deionized water. The preparation method follows the aforementioned method, and the deionized water is added when mixing photocurable PEGDA matrix and conductive PEDOT:PSS fillers.

2.3 Electrical field-assisted heterogeneous material printing

In the EF-HMP, the photocurable polymer matrix containing copper ion was solidified to form a two-dimensional (2D) pattern under the light beam projected from the optical system (refer Fig.1c and d). The digital model designed by SolidWorks was sliced to get a series of mask images, and then 2D light beam was projected layer by layer onto the surface of photocurable electrolyte solution to build 3D objects with complex structures. To fabricate metallic structures, the pre-printed part was lifted to make sure only the

surface of which required metal deposition was in contact with the solution. Then the electrical field was turned on, and the whole printed part acted as a cathode. Meanwhile, two copper electrodes (20×50mm) were placed in the glass tank and energized as anode for subsequent electrodeposition. During the electrodeposition, the anode continuously generated copper ions, and the copper ions moved to the surface of the printed polymer matrix to obtain electrons and form copper particles. To demonstrate the feasibility and capability of the proposed EF-HMP process, ASU pitchfork and a flexible electrical circuit were printed out. The layer thickness was 0.2 mm and the exposure time was 12 mins. The time and voltage of electrodeposition were 5 mins and 15V, respectively.

2.4 Rheological analysis and morphology characterization

The rheology of the photocurable electrolyte solutions was measured by DISCOVERY HR-30 rheometer (TA Instruments). The rotating element adopts a parallel plate with a diameter of 40 mm and a measurement gap of 1000 μ m. Viscosity was evaluated based on Cox-Merz rule and power-law in the frequency shear mode at room temperature (25°C) with shear rates ranging from 0.1 s⁻¹ to 1000 s⁻¹. The JEOL JXA-8530F electron microprobe analyzer was used to take morphological images of 3D printed pure polymer and the metallic deposition of copper.

2.5 Resistivity Evaluation

The resistivity of the solid part fabricated with developed photocurable electrolyte solutions at different ratio of PEDOT:PSS were studied by applying Ohm's law. A series of

rectangle sheets (15 × 3 × 1mm) was printed using the solation with various percentages of PEDOT:PSS for the resistivity test. The electrical resistivity ρ were calculated by the following equation [18]:

$$\rho = \frac{RA}{L} \tag{1}$$

where R is the resistance between the two endpoints of the solid rectangle; L is the length of the solid rectangle; A is the cross-sectional area of the solid rectangle. The length and cross-section area of the printed samples for the test is 15 mm and 3 mm², respectively.

2.6 Simulation of metal deposition under electrical field

In order to reduce the influence of proton concentration on copper deposition under the electrical field, the model chooses to simulate the deposition process at pH 4 using COMSOL Multiphysics. For this reason, the mass balance of protons does not need to be modeled, and sulfate is also regarded as a completely free ion. We assumed that the occurrence rate of deposition at the cathode and the dissolution at the anode is 100%, where the model completely excludes possible side reactions and there is no charge loss. A difference in electrolyte density occurs during the metal growth, resulting in a higher density at the anode than at the cathode. However, the free convection can be ignored because the change of components is minimal under the conditions of this modeling. The metal deposition process is inherently time-dependent, as it can be seen from the simulation results that the cathode boundary will change as the deposition occurs. Therefore, the Level-Set interface is used to track the cathode surface during the deposition process and automatically establishes the interface motion equation between

the liquid electrolyte and the solid electrode. Even PEDOT:PSS exists as conductive fillers in the form of solid particles, its influence on the movement of copper particles can be ignored. For simplicity, the composition of the electrolyte solution is a mixture of PEGDA and 1mol/L CuSO₄ solution with a ratio of 1:1. The metal deposition on the flat surfaces with and without a bump was simulated to evaluate the influences of the geometry of the printed part on the metal growth and deposition.

3 RESULTS AND DISCUSSION

3.1 EF-HMP of polymeric material with metallic structures

In EF-HMP, the dynamic electrical field was integrated with microscale mask image projection-based stereolithography (MIP-SL) (Fig.1c) [19]. The printing system is mainly composed of the optical projection system, electrical field generation and control module, material and platform, and linear motion module. To generate 2D patterned light beam, the white light with intensity of a 2500 lm was reflected by a digital micromirror device (DMD) comprised of a 1920×1080 array of micromirrors, and the brightness of each pixel in the projected light beam was controlled by adjusting the angle of the corresponding micromirror in the DMD. The reflected light was further focused by an achromatic objective lens (purchased from Thorlabs Inc.) with a focus distance f = 10mm. The largest projection area in this printing system was 34×25.5 mm, and the resolution of the projected light beam was $23.6 \,\mu\text{m/pixel}$. The printing platform on the Z axis lifted the solidified part and left space for the solution to refill. The electrical field generation system consisted of two parallel anode copper sheets and a cathode attached to the

235

236

237

238

239

240

241

242

243

244

245

246

247

248

249

250

251

252

253

254

255

printing platform (Fig.1d). A DC power source was used to generate an electric field between anode and cathode for subsequent electrical assisted metal deposition. The glass tank was coated with PDMS film to get a horizontal flat surface in order to avoid curing uneven layers. Besides, the PDMS film can reduce the peeling force and increase the surface roughness of the cured part, which was important for a further metal deposition because it can improve the adhesion of metal particles and the conductivity of the surface.

As shown in Fig.1e and f, the polymer and metal structures can be selectively printed at room temperature by controlling the electric field and light source. Specifically, when the light source is turned on and the electric field is turned off, photocurable PEGDA is solidified after UV light exposure. The chain-growth photopolymerization of PEGDA is initiated by absorption of ultraviolet light, and PEDOT:PSS and copper sulfate are enclosed during the crosslinking of the polymer chain. In terms of metal fabrication, the preprinted part is lifted until only the surface where the metal needs to be printed contacts with the printing solution. Then the light source is turned off, and the electric field is turned on. Since the electrode we used here is copper, copper particles gradually grew on the surface of the printed part until the electrical field is turned off. During the metal printing process, the copper plate at the anode loses two electrons under oxidation and becomes copper cations Cu²⁺, which dissolve in the polymer-based electrolyte solution. The copper cations in the solution are reduced to metallic copper particles at the cathode by gaining two electrons and accumulating on the surface of the preprinted part. By accumulating the polymer and metal layer by layer, the 3D shape can be formed. Hence, EF-HMP enables

257

258

259

260

261

262

263

264

265

266

267

268

269

270

271

272

273

274

275

276

277

the metal and polymer fabrication in the single process with a photocurable conductive solution at room temperature by controlling the electrical field and light exposure, which effectively avoids the tedious multiple manufacturing processes.

The printing results of thin film composited of polymer and metal are demonstrated in Fig.1g and h. The film with a size of 8 × 8 mm was cured, and half of the film contains a copper layer. To print the copper layer, the electrical field with the strength of 2.5 mA/mm² was turned on for 15 mins. The boundary of the copper and polymer is obvious, and it confirms that our developed photocurable electrolyte solution can be solidified to form the polymer matrix, and it also can be used for bulk copper deposition. The SEM characterization of the deposited copper layer reveals that the printed copper particles are attached to the surface of the polymer matrix in the form of coarse grains with a diameter of about 2 µm while the morphology of the polymer matrix is much smoother. The process planning of EF-HMP is shown in Fig.2a. The printing process starts with slicing the designed digital CAD model to generate a set of mask images using in-house software [20]. During the slicing, the material index of each layer is also stored with the generation of mask images. The layer containing metal will be marked as 1, and the corresponding area of the mask image will be turned to be black. When the slicing process is finished, the mask images are loaded into the printing operation software to form a 2D light beam with the desired pattern. Before the fabrication, the printing platform will move to the initial position. In order to initialize the position of the printing platform, the platform is lowered to just touch the upper surface of the top surface of the PDMS coated

on the solution tank. The printing platform is then raised by 200 µm, and the initial

exposure time of the 2D light beam is set at 16 mins to obtain the base layer, which helps eliminate voids or intrusion into the film during initialization. In term of subsequent printing parameter for the regular polymer layers, the layer thickness and exposure time of the 2D light beam are set at 200 µmm and 12 mins, respectively. After one layer is completely cured, the platform rises by 2mm and then drops by 1.8mm so that a new layer of material is formed under the force of vacuum and squeezing. To print metal layer, the printing platform is moved up and electrical field is turned on so that the copper is deposited onto the bottom surface of the printed part. Specifically, one layer of polymeric structure with the same pattern as the metal layer needs to be printed to control the shape of the metallic layer. When the printed sample is moved up, only the bottom surface of the preprint layer contacts with the printing solution so that the metal can grow on the contact area to form the desired shape. The cyclical iteration printing process stops after the designed model is printed. As shown in Fig.2b, a fork was printed using the aforementioned process.

3.2 Investigation of curing characteristics

The curing characteristics of the photocurable electrolyte solution with different percentage of PEDOT:PSS was studied to get a fundamental understanding of the effect of fillers on the curing of polymer-based solution. As shown in Fig.3a, the fiber-like PEDOT:PSS are uniformly distributed in the PEGDA matrix. The 2D light pattern is projected onto the solution's surface to solidify a particular area. The light beam of each pixel in the projection light follows the Gaussian function [21]. The curing depth of

photocurable material is determined by the light penetration depth and light exposure energy. The relationship between the cure depth C_d and energy input E_{max} is defined by the Beer-Lamber's equation [22]:

$$C_d = D_p \ln \left(\frac{E_{\text{max}}}{E_C} \right) \tag{2}$$

where D_p is the penetration depth of UV light into a photocurable solution until a reduction in irradiation of 1/e is reached; E_{max} is the peak exposure of light shining on the photocurable solution surface at the center area; and E_c is the minimum energy for the photocurable solution to be solidified.

The concentration of the PEDOT:PSS directly influences the curing parameter since the PEDOT:PSS particles scatter the projected light and further hinder the photopolymerization process. The characterization of the photocurable electrolyte solution gives us an intuitive insight to choose the suitable concentration of PEDOT:PSS for printing. The viscosity of the printing solution rises up dramatically with the increase of concentration of PEDOT:PSS (Fig.3b). The viscosity of the printing solution jumped to 1933.1 Pa·s when the concentration of PEDOT:PSS was increased to 3 wt %. However, if the viscosity of printing solution is greater than 1000 Pa·s, the material is hard to refill back to the fabrication area for the next layer fabrication by only using atmosphere pressure and the material gravity and it requires extra tools to achieve the material refilling [17]. Moreover, the solution becomes unsuitable for EF-HMP printing because the low fluidity and high viscosity resistance make the copper cations Cu²⁺ challenging to transport. Hence, different concentrations of PEDOT:PSS needs to be tried and screened

out a suitable concentration for printing, as the solution must be suitable not only for curing but also for the electrical assisted deposition.

As shown in Fig.3c, the curing depth decreased gradually as the concentration of PEDOT:PSS was increased, which was caused by the light-shielding properties of the increasingly aggregated PEDOT:PSS. For example, the cure depth of the printing solution decreased from 320 μ m to 140 μ m when the concentration of PEDOT:PSS was increased to 10 wt%. The curing depth of the printing solution after adding the PEDOT:PSS can be determined by Griffith and Halloran, using the following equation [23, 24]:

$$C_d = \left(\frac{\eta_0}{\eta_P - \eta_0}\right) \frac{\lambda^2}{d} \ln\left(\frac{t}{t_c}\right) \frac{1}{\varphi} \tag{3}$$

where η_0 is the refractive index of the photocurable PEGDA resin, η_P is the refractive index of the PEDOT:PSS, λ is the wavelength of light in nm, d is diameter of the PEDOT:PSS particles, t is the exposure time, t_c is the critical exposure time, and φ is the concentration of PEDOT:PSS particles.

Furthermore, when the concentration of PEDOT:PSS exceeds 5 wt%, the curing depth of the solution was reduced but not as drastically as it increased from 1 wt% to 5 wt%. In contrast, the viscosity of the solution increased sharply (Fig. 3b). This is because 2 wt% of the PEDOT:PSS can homogeneously suspend inside the PEGDA based solution, and the printing solution had flowability. While the solution behaved like a slurry when the concentration of PEDOT:PSS increased to 10 wt%. Since the viscosity of PEDOT:PSS based printing solution with a proportion larger than 3 wt% has far exceeded 1000 Pa·s, which

is not easy to fabricate metal layer by using our EF-HMP process, only the solution with a ratio of PEDOT:PSS less than 3% can be selected as the potential printing materials.

The relationship between the exposure time of the photocurable electrolyte solution and the concentration of PEDOT:PSS is shown in Fig.3d. For example, the exposure time increased slightly as the concentration of PEDOT:PSS increased from 1 wt% to 3 wt%. Once the concentration of PEDOT:PSS exceeded the threshold of 5 wt%, the curing time of the printing electrolyte solution increased drastically. For example, the exposure time required 45s to solidify the printing electrolyte solution with 3 wt% PEDOT:PSS while it takes nearly 8 times longer (350s) to cure the 5 wt% PEDOT:PSS solution. This is because when the concentration of PEDOT:PSS was larger than 3 wt%, the PEDOT:PSS aggregated into large particles, which absorbed and scattered most of light.

3.3 Investigation of metallic structures growth

After the curing performance of the printing electrolyte solution was studied, the growth of the metallic structures was further investigated. To study the feasibility and effectiveness of the metal deposition under the electrical field using the photocurable electrolyte solution proposed in this paper, the fabrication performance of metallic structures using EF-HMP was evaluated quantitatively by calculating the thickness of the deposition, which is discussed in this section. Theoretically, the thickness of the newly grown has a linear relationship with the electrical current density (voltage) and the growth time. The relationship among the growth thickness of metallic structures,

379

380

electrical field parameters, and the deposition area is given by the following theoretical calculation formula [25]:

$$Q = J \times S \tag{4}$$

- where *Q* indicates the amount of electricity, which reflects the growth thickness of the metallic structures on the polymer; *J* is the current density of the electrical field; and *S* is the area of the deposition.
- To further simplify the calculation, an empirical formula was used to calculate the growth thickness of metallic structures [25]:

$$T = J \times t_0 \times \eta \times 0.0202 \tag{5}$$

- where T indicates the layer thickness of the newly deposited copper particles; J is the current density of the electrical field; t_0 is the deposition time; and η is the deposition efficiency, 95% used in this work.
- According to the Faraday's law, the weight of material liberated or deposited at the anode and cathode is proportional to the electrical quantity, and the equation is thus given by [25]:

$$m = \frac{QF}{Mz} \tag{6}$$

where m is weight of material liberated at the anode; Q is the electrical quantity passed through anode; F=96485 C/mol is the Faraday constant; M is the molar mass of material at the anode; and z is the valence number of ions of the material at the anode.

382

383

384

385

386

387

388

389

390

391

392

393

394

395

396

397

398

399

400

401

402

The physics-assisted simulation was conducted to study the quality of metallic structures printed by the EF-HMP process. The simulation results demonstrate that the copper particles gradually adhere to the pre-cured polymer-based part to form a thin layer with uniform thickness under the electric field, as visible from the brown area in Fig.4. The simulation of the forming process of the metallic structures on the flat surface plating showed that the thickness of the plating layer gradually increases to 0.83 µm at 15s, and electrical potential near the surface evenly decreases (Fig.4a). The forming process of the metallic structures on the complex 3D shape such as a convex surface with the bump is shown in Fig.4b. The top surface of the bump turned out to be thicker than the one of other places due to the uneven coating thickness. The unevenness forming of the metallic structures on the bump will directly affect the distribution of the electric potential and further strengthen the non-uniformity of the metallic structure's growth. Therefore, the uneven growth of the metallic structures needs to be controlled by adjusting the deposition time during printing of the metal layer. Besides, the geometry of the model can be optimized to avoid sharp boundary transitions. In addition, the simulation results show that there is a significant change in the concentration of copper cations Cu²⁺ in the solution near the deposition area, which is consistent with the amount of copper particles deposited on the surface.

As depicted in Fig.5a, the growth process of metallic structures occurs because of the following simplified mechanism. The copper in the anode firstly loses electrons to become copper cations Cu²⁺ and copper cations Cu²⁺ further move to the cathode surface to obtain electrons and form the copper particles. For electroplating of copper, oxidation

and reduction take place at anode and cathode, which can be expressed as the following equations.

405 The ionization of copper at anode:

$$Cu(s) - 2e^- \rightarrow Cu^{2+}(aq) \tag{7}$$

407 The deposition of copper at cathode:

408
$$Cu^{2+}(aq) + 2e^{-} \rightarrow Cu(s)$$
 (8)

The newly grown copper particles are attached to the surface of the polymer matrix in the form of grains, which can be seen by SEM morphology characterization (Fig.1e and f). The efficiency of the electrical assisted metal deposition is closely related to the conductivity of the cured polymer. The lower resistance makes the copper cations Cu^{2+} get electrons and deposit more quickly. The quantitative analysis of the conductivity of the EH-HMP printed polymer is shown in Fig.5b. The resistivity decreases logarithmically with the increase of the concentration of PEDOT:PSS. For instance, the resistivity of the solution with 2 wt% of PEDOT:PSS is 615.4 K Ω ·mm, which is half of that of the solution with 1 wt%, but 34 times of that of the solution contains 5 wt% of PEDOT:PSS. Since the viscosity of the solution with 3 wt% of PEDOT:PSS is too high to print using EF-HMP, the solution with 2 wt% of PEDOT:PSS was used to print the sample parts.

The electrical field-assisted metal deposition performed by the photocurable electrolyte solution indicates a high correlation among deposition thickness, electrical charge and deposition time. To identify the relationship between deposition thickness and different voltages, a series of voltages ranging from 3V to 30V were used in the

425

426

427

428

429

430

431

432

433

434

435

436

437

438

439

440

441

442

443

444

445

applied voltage is less than 5V (refer Fig.5c). There was not enough potential difference to continuously initiate the electron transfer required for electrical field-assisted metal deposition to obtain a thicker coating. However, once the applied voltage exceeded a certain threshold, the deposition thickness of copper increased significantly. For example, the deposition thickness of copper raised from 50 µm at 25V to 90 µm at 30V when the deposition time was 5 mins. However, the excessively high voltage will generate side effects that make the water inside the solution electrolyzed and this reaction plays a dominant role. This is because the movement speed of the copper cations Cu²⁺ in the highviscosity solution is limited. In addition, the heat generated during the electrical fieldassisted metal deposition process will gradually make the cured part lose water and further reduce its conductivity, which makes it incapable of deposition. In terms of the deposition time, the deposition thickness of copper at different depositing times under 15V is shown in Fig.5d. The thickness increased from 30 μm at 1 min to 90 μm at 25 mins. However, the thickness turned out to be the same after 25 mins and the formed copper particles were suspended in the printing solution near the deposition area. This is because the newly deposited copper particles cannot effectively adhere to the surface of the predeposited copper layer on the solidified polymer part. After the investigation of the printing parameters, three demo parts, including a pitchfork (Fig.6a), a "polymer-metal-polymer" sandwich structure (Fig.6f), and a circuit (Fig.6h) were fabricated to show the print capability and accuracy of the proposed EF-

HMP process. As shown in Fig.6b and c, the pitchfork was cured layer by layer on the base

experiments. After 5 mins, the deposition thickness of copper can be 10 µm when the

layer, which was designed to make the cured layer better adhere to the printing platform. The sharp edges and corners of the printed pitchfork are visible, and the width of the narrowest area is a few hundred microns. After the fabrication of polymer layers, the light source was turned off, and the electrical field was turned on for 5 mins at 15V. Using the same printing solution, a thin layer of copper grew on the surface of the last layer of the printed pitchfork. The thickness of the deposited copper can be directly seen from Fig.6d, and it was about 45 μ m, which is consistent with the previous data summarized in Fig.5d. With regard to the microscopic morphological distribution of the deposited copper, numerous copper particles with a size of a few microns are uniformly attached to the polymer surface, as shown in Fig.6e.

A triangle-shaped "polymer-metal-polymer" sandwich structure was designed and printed to show the multilayer fabrication capability of the EF-HMP process (Fig.6f and g). The base triangle of polymeric material was firstly printed using 0.1 mm layer thickness and 75 s per layer exposure time. Then a layer of middle-sized triangle-shaped polymeric material was built for the growth of the metal layer. The electrical field (15 V) was applied to the printing area, and copper particles gradually grew on the surface of the polymeric material. After 5 mins, the electrical field was turned off and a 50 μ m copper layer was successfully printed on the surface of the polymer. Then a smaller triangle light beam was projected at the printing area. The liquid polymeric material between the PDMS film and the copper layer was solidified to form the top polymeric layer of the sandwich structure with a 0.8 mm thickness.

Furthermore, EF-HMP process can be used to print a flexible circuit. For example, the conductive circuit consisting of a LED light and copper/polymer-based lines were designed fabricated using a single step. As shown in Fig.6h, the lower ends of the polymer lines are connected to the DC power supply (5V). When the two poles of the LED light touched the upper end of the line without the copper layer, the LED didn't light up (Fig.6i). When the circuit line was printed with copper layer, the circuit was turned on, and the LED lighted up (Fig.6j). Experimental results of conductive circuit show its broad prospects in the fabrication of polymer/metal devices for the applications such as sensor, antenna, and integrated circuits with complex shape accuracy.

4 CONCLUSION

In this work, an electrical field-assisted heterogeneous material printing (EF-HMP) method has been developed to fabricate polymer materials with metallic structures using PEGDA and PEDOT:PSS polymer-based photocurable and conductive composite. We successfully prepared photocurable electrolyte composite and further investigated the printability and electrical field-assisted deposition performance. The influences of the percentage of the PEDOT:PSS on the curing characteristics, viscosity, resistance, and metallic structure growth were studied. Based on the experimental results, photocurable electrolyte composite with 2 wt% of PEDOT:PSS showed superior curing properties, and it can also promote the metal deposition inside the electrical field. Moreover, the 3D printed metallic structures exhibit excellent shape accuracy and conductivity. The proposed EF-HMP process provides a novel manufacturing tool for the fabrication of the

scaly-foot snail inspired polymer/metal structures at room temperature using a single process. It enables broad application prospects in manufacturing polymer/metallic hierarchical structures. We believe the study on the preparation of photocurable electrolyte composite and the electrical field-assisted printing method gives insights on the improvement of the manufacturing efficiency and costs in the field of heterogeneous material manufacturing. In the future, the bonding adhesion between metallic structures and polymer will be studied and objects with more complex material distribution will be printed. Moreover, the properties enhancement of bioinspired heterogeneous material structures will be studied by using the proposed printing method.

ACKNOWLEDGMENT

The authors acknowledge the ASU core research facilities for the use of SEM electron microprobe analyzer, and Prof. Kailong Jin's Lab for the use of the viscosity testing machine.

FUNDING

The authors acknowledge ASU startup funding, and National Science Foundation (NSF grant No. CMMI-2114119).

508 **NOMENCLATURE**

AM additive manufacturing

3D three dimensional

SL stereolithography

FDM fused deposition modelling

PLA polylactic acid

DIW direct ink writing

HAE hydrogen assisted electroplating

EF-HMP electrical field-assisted heterogeneous material printing

MIP-SL mask image projection-based stereolithography

DMD digital micromirror device

PEDOT:PSS poly(3,4-ethylenedioxythiophene)-poly (styrenesulfonate)

PEGDA poly(ethylene glycol) diacrylate

2D two dimensional

SEM scanning electron microscopy

ρ electrical resistivity

R resistance

L length

A cross-sectional area

*C*_d curing depth

 D_p light penetration depth

E _{max}	peak light intensity
E_c	energy threshold for photocuring
η_0	refractive index of the photocurable PEGDA resin
$\eta_{\scriptscriptstyle P}$	refractive index of the PEDOT:PSS
λ	wavelength of light
d	diameter of the PEDOT:PSS particles
t	exposure time
t _c	critical exposure time
arphi	concentration of PEDOT:PSS particles
Q	electricity
J	current density
S	plating area
T	copper layer thickness
t_0	plating time
η	plating efficiency
m	weight of material
Q	electrical quantity
F	faraday constant
М	molar mass of material
Z	valence number of ions of the material

REFERENCES

511

- [1] Yang, Y., Song, X., Li, X., Chen, Z., Zhou, C., Zhou, Q., and Chen, Y., 2018, "Recent Progress in Biomimetic Additive Manufacturing Technology: From Materials to Functional Structures," Adv Mater, 30(36), p. e1706539. DOI: 10.1002/adma.201706539
- 516 [2] Yao, H., Dao, M., Imholt, T., Huang, J., Wheeler, K., Bonilla, A., Suresh, S., and Ortiz, C., 2010, "Protection mechanisms of the iron-plated armor of a deep-sea hydrothermal vent gastropod," Proc Natl Acad Sci, 107(3), pp. 987-992. DOI: 10.1073/pnas.0912988107
- 520 [3] Zhang, C., Li, X., Jiang, L., Tang, D., Xu, H., Zhao, P., Fu, J., Zhou, Q., and Chen, Y., 2021,
 "3D Printing of Functional Magnetic Materials: From Design to Applications,"
 522 Advanced Functional Materials, 31(34), p. 2102777. DOI: 10.1002/adfm.202102777
- [4] Yang, Y., Li, X., Chu, M., Sun, H., Jin, J., Yu, K., Wang, Q., Zhou, Q., and Chen, Y., 2019, "Electrically assisted 3D printing of nacre-inspired structures with self-sensing capability," Science Advances, 5(4), p. eaau9490. DOI: 10.1126/sciadv.aau9490
- 526 [5] Joralmon, D., Alfarhan, S., Kim, S., Tang, T., Jin, K., and Li, X., 2022, "Three-527 Dimensional Printing of Liquid Crystals with Thermal Sensing Capability via 528 Multimaterial Vat Photopolymerization," ACS Applied Polymer Materials, 4(4), pp. 529 2951-2959. DOI: 10.1021/acsapm.2c00322
- 530 [6] Li, X., Yang, Y., Xie, B., Chu, M., Sun, H., Hao, S., Chen, Y., and Chen, Y., 2019, "3D printing of flexible liquid sensor based on swelling behavior of hydrogel with carbon nanotubes," Advanced Materials Technologies, 4(2), p. 1800476. DOI: 10.1002/admt.201800476
- 534 [7] Seol, S. K., Kim, D., Lee, S., Kim, J. H., Chang, W. S., and Kim, J. T., 2015, 535 "Electrodeposition-based 3D printing of metallic microarchitectures with controlled 536 internal structures," Small, 11(32), pp. 3896-3902. DOI: 10.1002/smll.201500177
- 537 [8] Zhu, Y., Tang, T., Zhao, S., Joralmon, D., Poit, Z., Ahire, B., Keshav, S., Raje, A. R., Blair, 538 J., and Zhang, Z., 2022, "Recent Advancements and Applications in 3D Printing of 539 Functional Optics," Additive Manufacturing, p. 102682. DOI: 540 10.1016/j.addma.2022.102682
- 541 [9] Wang, X., Jiang, M., Zhou, Z., Gou, J., and Hui, D., 2017, "3D printing of polymer matrix 542 composites: A review and prospective," Composites Part B: Engineering, 110, pp. 442-543 458. DOI: 10.1016/j.compositesb.2016.11.034
- [10] Hudkins, J. R., Wheeler, D. G., Peña, B., and Berlinguette, C. P., 2016, "Rapid prototyping of electrolyzer flow field plates," Energy & Environmental Science, 9(11), pp. 3417-3423. DOI: 10.1039/C6EE01997H
- [11] Rosa-Ortiz, S. M., Kadari, K. K., and Takshi, A., 2018, "Low temperature soldering surface-mount electronic components with hydrogen assisted copper electroplating," MRS Advances, 3(18), pp. 963-968. DOI: 10.1557/adv.2017.641
- [12] Lazarus, N., Bedair, S. S., Hawasli, S. H., Kim, M. J., Wiley, B. J., and Smith, G. L., 2019, "Selective Electroplating for 3D - Printed Electronics," Advanced Materials Technologies, 4(8), p. 1900126. DOI: 10.1002/admt.201900126

- 553 [13] Angel, K., Tsang, H. H., Bedair, S. S., Smith, G. L., and Lazarus, N., 2018, "Selective 554 electroplating of 3D printed parts," Additive Manufacturing, 20, pp. 164-172. DOI: 555 10.1016/j.addma.2018.01.006
- [14] Hensleigh, R., Cui, H., Xu, Z., Massman, J., Yao, D., Berrigan, J., and Zheng, X., 2020,
 "Charge-programmed three-dimensional printing for multi-material electronic devices," Nature Electronics, 3(4), pp. 216-224. DOI: 10.1038/s41928-020-0391-2
- [15] Zhao, Z., Bai, J., Yao, Y., and Wang, C., 2020, "Printing continuous metal structures via
 polymer-assisted photochemical deposition," Materials Today, 37, pp. 10-17. DOI:
 10.1016/j.mattod.2020.03.001
- [16] Yang, X., Sun, M., Bian, Y., and He, X., 2019, "A Room Temperature High Conductivity Metal Printing Paradigm with Visible Light Projection Lithography,"
 Advanced Functional Materials, 29(1), p. 1807615. DOI: 10.1002/adfm.201807615
- [17] Warr, C., Valdoz, J. C., Bickham, B. P., Knight, C. J., Franks, N. A., Chartrand, N., Van
 Ry, P. M., Christensen, K. A., Nordin, G. P., and Cook, A. D., 2020, "Biocompatible
 PEGDA Resin for 3D Printing," ACS Appl Bio Mater, 3(4), pp. 2239-2244. DOI:
 10.1021/acsabm.0c00055
- [18] McLachlan, D. S., Blaszkiewicz, M., and Newnham, R. E., 1990, "Electrical resistivity of composites," Journal of the American Ceramic Society, 73(8), pp. 2187-2203. DOI: 10.1111/j.1151-2916.1990.tb07576.x
- 572 [19] Li, X., Mao, H., Pan, Y., and Chen, Y., 2019, "Mask video projection-based 573 stereolithography with continuous resin flow," Journal of Manufacturing Science and 574 Engineering, 141(8), p. 081007. DOI: 10.1115/1.4043765
- [20] Li, X., Xie, B., Jin, J., Chai, Y., and Chen, Y., 2018, "3D printing temporary crown and
 bridge by temperature controlled mask image projection stereolithography,"
 Procedia Manufacturing, 26, pp. 1023-1033. DOI: 10.1016/j.promfg.2018.07.134
- [21] Li, X., Baldacchin, T., Song, X., and Chen, Y., 2016, "Multi-scale additive manufacturing: an investigation on building objects with macro-, micro-and nanoscales features," 11th International Conference on Micro Manufacturing, Irvine, CA, Mar, p. 96.
- 582 [22] Jacobs, P. F., 1992, Rapid prototyping & manufacturing: fundamentals of stereolithography, Society of Manufacturing Engineers.
- [23] Joyee, E. B., Lu, L., and Pan, Y., 2019, "Analysis of mechanical behavior of 3D printed heterogeneous particle-polymer composites," Composites Part B: Engineering, 173, p. 106840. DOI: 10.1016/j.compositesb.2019.05.051
- [24] Yasui, M., and Ikuta, K., 2017, "Modeling and measurement of curing properties of photocurable polymer containing magnetic particles and microcapsules," Microsyst Nanoeng, 3(1), p. 17035. DOI: 10.1038/micronano.2017.35
- 590 [25] Schlesinger, M., and Paunovic, M., 2011, Modern electroplating, John Wiley & Sons.
- [26] Chen, C., Uematsu, K., Linse, K., and Sigwart, J. D., 2017, "By more ways than one:
 rapid convergence at hydrothermal vents shown by 3D anatomical reconstruction of
 Gigantopelta (Mollusca: Neomphalina)," BMC evolutionary biology, 17(1), pp. 1-19.
 DOI: 10.1186/s12862-017-0917-z

Figure Captions List

Fig. 1 Schematic diagram of electrical field-assisted heterogeneous material printing for the construction of polymeric material with metallic structures. (a) Photograph of the scaly-foot snail (copyright from [26]); (b) multi-layer structures of the shell cross section (copyright from [2]); (c) schematic diagram of the EF-HMP set-up; (d) illustration of optical projection and electrical field generation in the EF-HMP process; (e) schematic diagram of the curing process and the crosslinking initiated by photopolymerization; (f) schematic diagram of the electrical field assisted metal deposition; (g) optical and scanning electron microscopy (SEM)

Fig. 2 Schematic diagram of the EF-HMP of 3D objects consist of metallic structures and polymer. (a) process planning of the EF-HMP; and (b) diagrams of the fabrication process and the result of the ASU pitchfork including slicing, projection images, 2D light beam, and the fabrication result.

images of EF-HMP printed polymer; and (h) metallic structures.

of the projection light penetrates the material; (b) viscosity characterization of the photocurable electrolyte solution with concentrations of PEDOT:PSS from 1 wt% to 10 wt%; and (c) the corresponding curing depth; and (d) exposure time. Each error bar

represents the original data ranges 5% above and below the mean from at least 5 data points.

- Fig. 4 Simulation of metal deposition under the electrical field. (a) metal deposition on the flat surface; and (b) metal deposition on the convex surface under the electrical field.
- Fig. 5 Evaluation of the printed metallic structures under the electrical field. (a) schematic diagram of the metal deposition under the electrical field; (b) the resistivity of the cured polymer matrix-based part with different concentrations of PEDOT:PSS; (c) the relation between voltage and the deposition layer thickness when the deposition time is 5 mins; and (d) the relation between deposition time and the deposition layer thickness when the deposition voltage is 15V. Each error bar represents the original data ranges 5% above and below the mean from at least 5 data points.
- Fig. 6 Electrical field-assisted heterogeneous material printing (EF-HMP) of polymeric material with metallic structures for different applications. (a) Schematic diagram of pitchfork model; (b) the EF-HMP printed polymer pitchfork; (c) the polymer pitchfork printed with copper layer; (d) morphology characterization of the cross-section area of (c); (e) morphology characterization of copper layer; (f) CAD model of a "polymer-metal-polymer" sandwich structure; (g) microscope images of the printed

sandwich structure; (h) circuit conductivity demonstration, and the circuit made by (i) pure polymer; and (j) pure polymer with a copper layer.

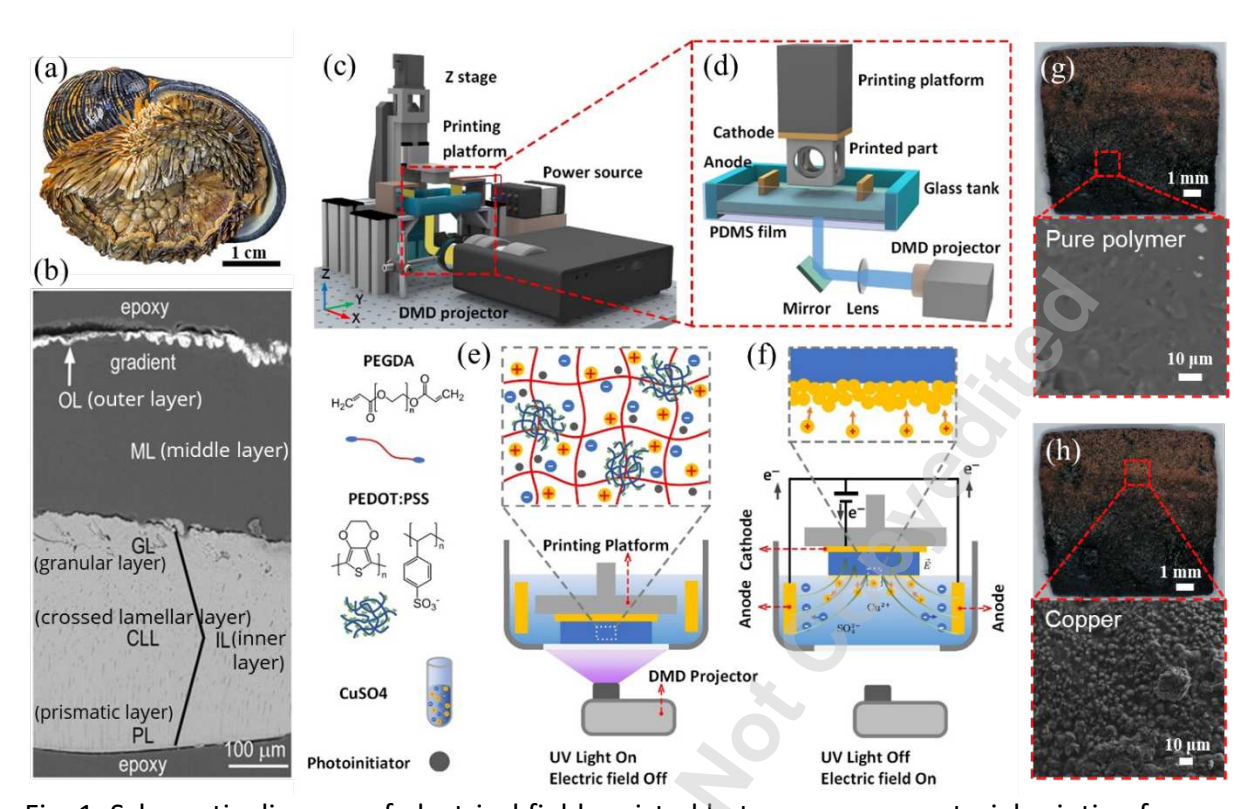


Fig. 1 Schematic diagram of electrical field-assisted heterogeneous material printing for the construction of polymeric material with metallic structures. (a) photograph of the scaly-foot snail (copyright from [26]); (b) multi-layer structures of the shell cross section (copyright from [2]); (c) schematic diagram of the EF-HMP set-up; (d) illustration of optical projection and electrical field generation in the EF-HMP process; (e) schematic diagram of the curing process and the crosslinking initiated by photopolymerization; (f) schematic diagram of the electrical field assisted metal deposition; (g) optical and scanning electron microscopy (SEM) images of EF-HMP printed polymer; and (h) metallic structures.

609

610

611

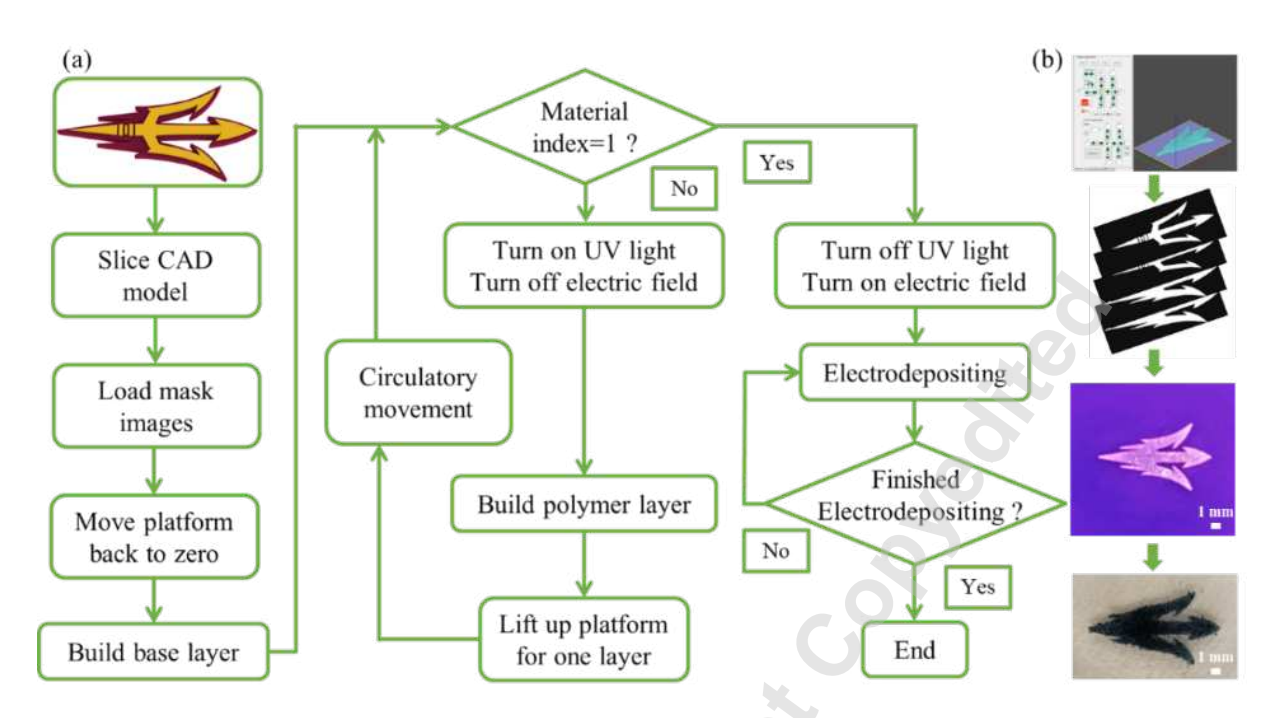


Fig. 2 Schematic diagram of the EF-HMP of 3D objects consist of metallic structures and polymer. (a) Process planning of the EF-HMP; and (b) diagrams of the fabrication process and the result of the ASU pitchfork including slicing, projection images, 2D light beam, and the fabrication result.

614

615

616

617

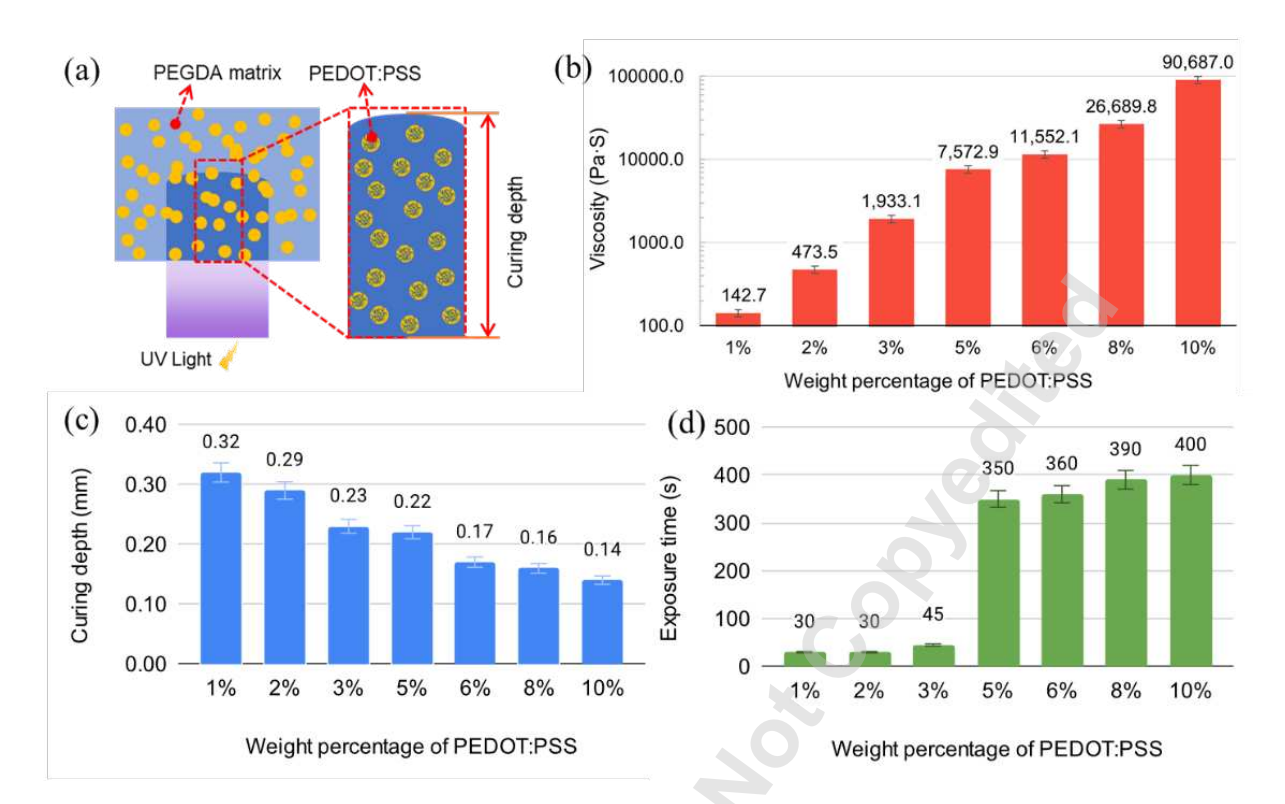


Fig. 3 Curing study of the photocurable plating solution. (a) Schematic diagram of the projection light penetrates the material; (b) viscosity characterization of the photocurable electrolyte solution with concentrations of PEDOT:PSS from 1 wt% to 10 wt%; and (c) the corresponding curing depth; and (d) exposure time. Each error bar represents the original data ranges 5% above and below the mean from at least 5 data points.

solution

t=0s

619

620

621

Cured film Cured film Cured film Cured film (a) Conductive Polymer solution t=5s t=10s t=15s t=0s Cured film Cured film Cured film Cured film Cured film (b) Conductive Polymer

t=6s

t=9s

t=12s

Fig 4: Simulation of metal deposition under the electrical field. (a) Metal deposition on the flat surface; and (b) metal deposition on the convex surface under the electrical field.

t=3s

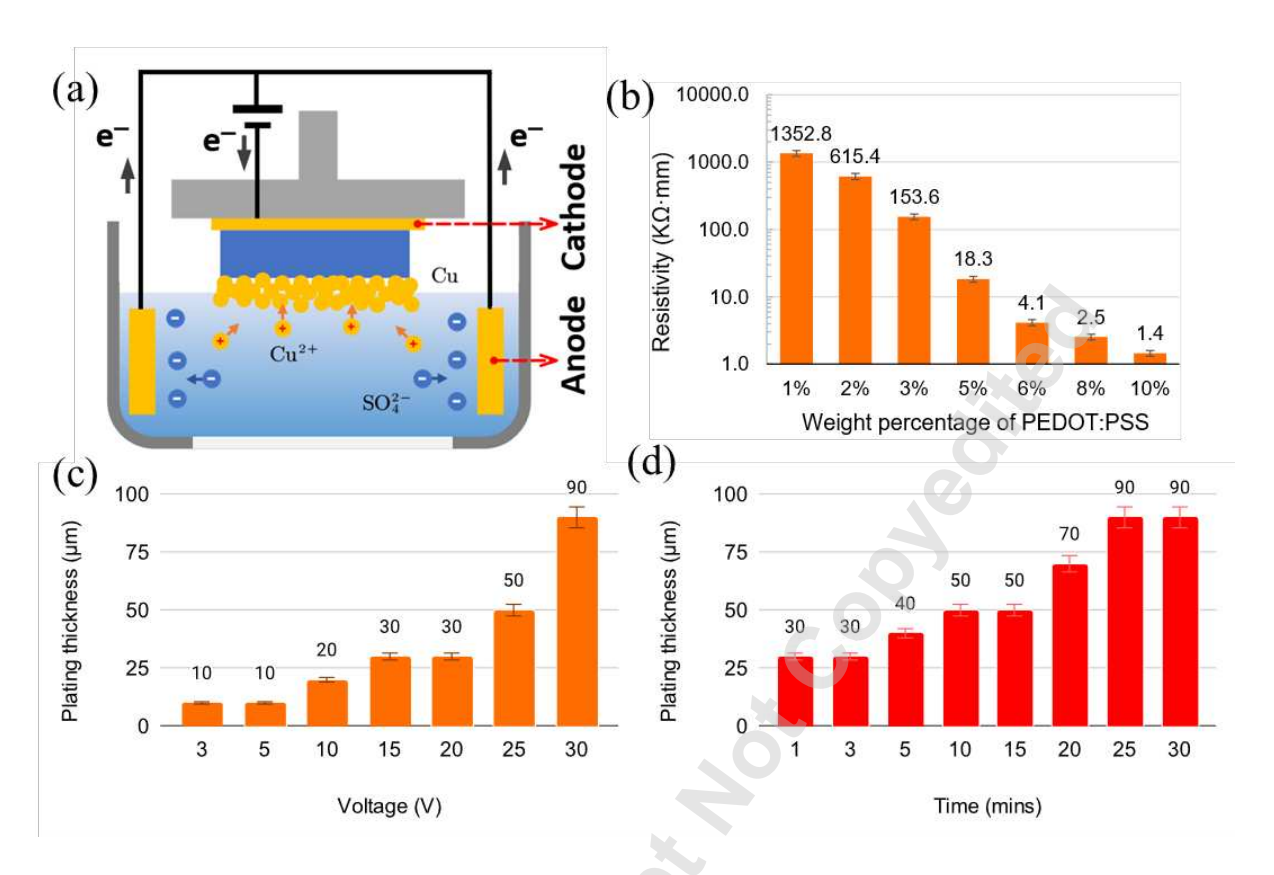


Fig. 5 Evaluation of the printed metallic structures under the electrical field. (a) Schematic diagram of the metal deposition under the electrical field; (b) the resistivity of the cured polymer matrix-based part with different concentrations of PEDOT:PSS; (c) the relation between voltage and the deposition layer thickness when the deposition time is 5 mins; and (d) the relation between deposition time and the deposition layer thickness when the deposition voltage is 15V. Each error bar represents the original data ranges 5% above and below the mean from at least 5 data points.

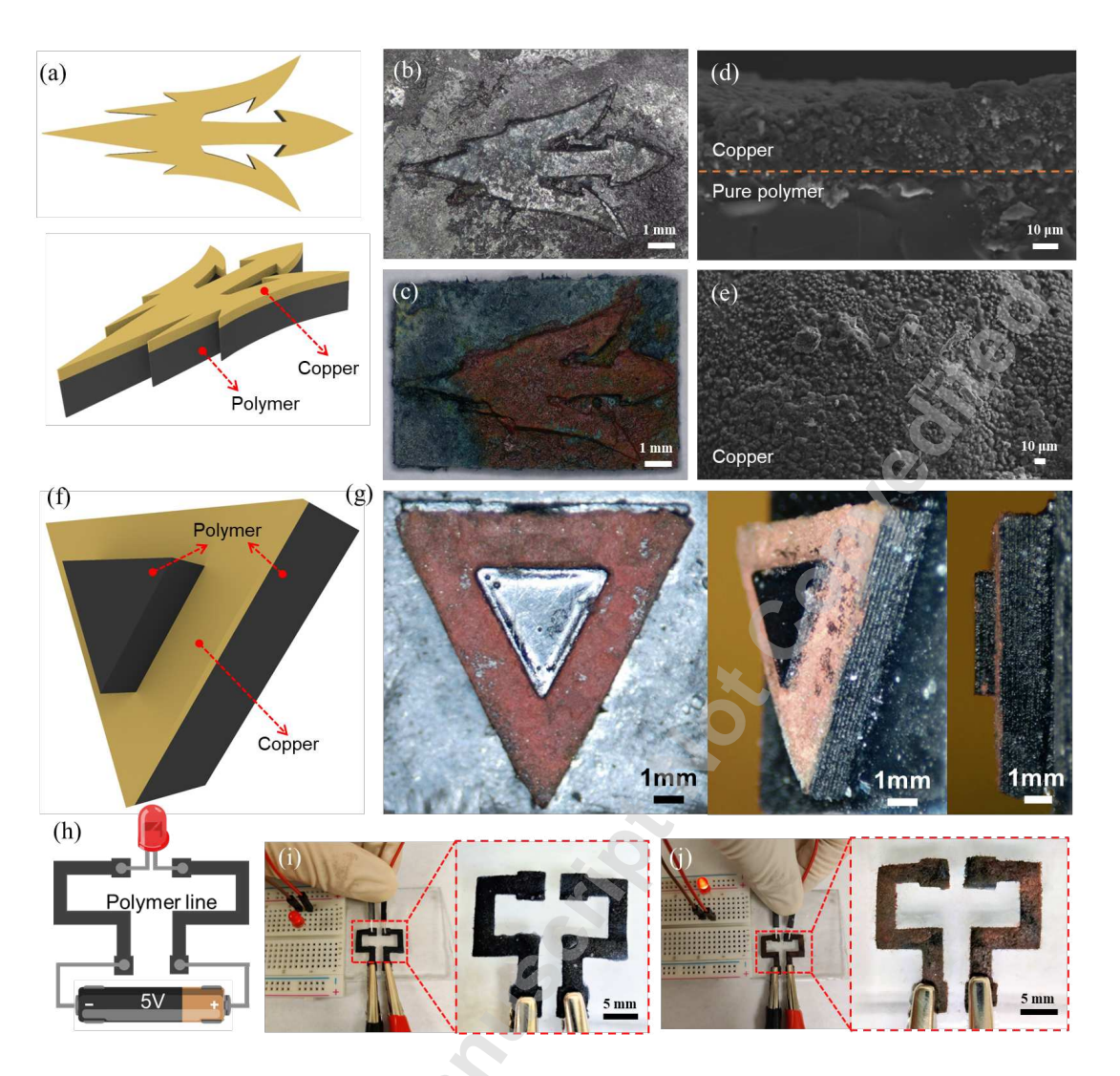


Fig. 6 Electrical field-assisted heterogeneous material printing (EF-HMP) of polymeric material with metallic structures for different applications. (a) Schematic diagram of pitchfork model; (b) the EF-HMP printed polymer pitchfork; (c) the polymer pitchfork printed with copper layer; (d) morphology characterization of the cross-section area of (c); (e) morphology characterization of copper layer; (f) CAD model of a "polymer-metal-polymer" sandwich structure; (g) microscope images of the printed sandwich structure; (h) circuit conductivity demonstration, and the circuit made by (i) pure polymer; and (j) pure polymer with a copper layer.